The Thermodynamic Landscape of Testosterone Binding to Cytochrome P450 3A4: Ligand Binding and Spin State Equilibria†

Arthur G. Roberts, A. Patricia Campbell, and William M. Atkins*

Department of Medicinal Chemistry, University of Washington, Box 357610, Seattle, Washington 98195-761

Received August 28, 2004; Revised Manuscript Received November 3, 2004

ABSTRACT: Human cytochrome P450 (CYP) 3A4 catalyzes the oxygen-dependent metabolism of greater than 60% of known drugs. CYP3A4 binds multiple ligands simultaneously, and this contributes to complex allosteric kinetic behavior. Substrates that bind to this enzyme change the ferric spin state equilibrium of the heme, which can be observed by optical absorbance and electron paramagnetic resonance (EPR) spectroscopy. The ligand-dependent spin state equilibrium has not been quantitatively understood for any ligands that exhibit multiple binding. The CYP3A4 substrate testosterone (TST) has been shown previously by absorbance spectroscopy to induce spin state changes that are characteristic of a low spin to high spin conversion. Here, EPR was used to examine the equilibrium binding of TST to CYP3A4 at [CYP3A4] > K_D, which allows for characterization of the singly occupied state (i.e., CYP3A4·TST). We also have used absorbance spectroscopy to examine equilibrium binding, where [CYP3A4] < K_D, which allows for determination of K_D's. The combination of absorbance and EPR spectroscopy at different CYP3A4 concentrations relative to K_D and curve fitting of the resultant equilibrium binding titration curves to the Adair−Pauling equations, and modifications of it, reveals that the first equivalent of TST binds with higher affinity than the second equivalent of TST and its binding is positively cooperative with respect to ligand-dependent spin state conversion. Careful analysis of the EPR and absorbance spectral results suggests that the binding of the second TST induces a shift to the high spin state and thus that the second TST binding causes displacement of the bound water. A model involving six thermodynamic states is presented and this model is related to the turnover of the enzyme.

The hepatic cytochrome P450s (CYPs)[1] catalyze the oxidative metabolism of toxins and drugs (*1*). As detoxification enzymes, the CYPs often demonstrate broad substrate selectivity and product diversity with many structurally unrelated substrates and inhibitors binding to a single CYP isoform. Several CYPs exhibit non-Michaelis−Menten steady-state kinetic behavior in vitro and possibly in vivo. (*2*−*7*). These complex kinetics include positive and negative homotropic and heterotropic allosterism, which is further complicated by the fact that the individual ligand can act as either an inhibitor or an activator, depending on which substrate is present (*7*, *8*). These allosteric kinetics confound prediction of in vivo metabolism based on in vitro kinetic data and, moreover, may contribute to drug−drug interactions. Therefore, a mechanistic understanding of CYP allosterism will improve prediction and understanding of drug metabolism and drug interactions in vivo.

An emerging paradigm concerning CYP allosterism is that multiple substrates (S) or effectors (E) can simultaneously occupy a single large active site and that the different properties of [CYP·S], [CYP·S·S], and [CYP·S·E] lead to allosteric kinetics (*2*, *7*, *9*). Due to the complexity of the CYP reaction cycle, which includes multiple intermediates, protein−protein complex formation, and abortive uncoupling reactions, it remains uncertain how the allosterism in steady-state kinetic experiments correlates with the cooperativity observed in the elementary steps of the reaction cycle including ligand binding, the ferric spin state equilibrium, heme reduction, and substrate oxidation. Notable progress in this area includes the demonstration that CYP2C9 is more "coupled" with less production of peroxide and water when flurbiprofen is present together with the substrate dapsone, presumably because flurbiprofen forces the substrate to bind in a more "productive" mode (*10*). Apparently, the branching ratio(s) for release or formation of reduced oxygen species vs substrate oxidation are altered upon binding of a second ligand or substrate. Based on this precedent, a complete understanding of CYP allosterism requires quantitative knowledge of the energetics of binding for each ligand state when multiple ligands bind.

Historically, many investigators have relied on ligand-dependent heme spin state conversion to monitor ligand binding. Specifically, many ligands displace water from the distal heme surface, resulting in the conversion of a six-coordinate, water-ligated, low spin heme iron to a five-

† This work was supported by National Institutes of Health Grants GM32165 and T32 07750 (J.T.P.) and the Center for Ecogenetics and Environmental Health from the National Institute of Environmental Health Sciences, University of Washington Center Grant No. P30ES07033.

* Corresponding author. Tel: (206) 685-0379. Fax: (206) 685-3252. E-mail: winky@u.washington.edu.

[1] Abbreviations: CYP, cytochrome P450; CYP3A4, human cytochrome P450 3A4; DMSO, dimethyl sulfoxide; E, effector; EPR, electron paramagnetic resonance; HS, high spin; K_{spin}, spin state equilibrium; L, ligand; LS, low spin; S, substrate; SDS−PAGE, sodium dodecyl sulfate−polyacrylamide gel electrophoresis; TST, testosterone; UV, ultraviolet; *Y*, fractional increase in absorbance at 390 nm.

10.1021/bi0481390 CCC: $30.25
Published on Web 01/07/2005

Scheme 1: Generic Model for Ligand-Dependent Spin State Equilibria of CYPs with Multiple Ligand Binding[a]

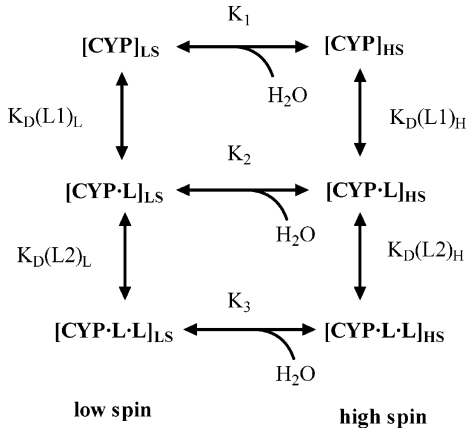

[a] The low spin and high spin states are represented by the subscripts LS and HS, respectively. L is a ligand, which according to this model can bind with a stoichiometry of 1 or 2 per CYP. The equilibrium constants for the relative fraction of high spin and low spin are $K_1 = [CYP]_{HS}/[CYP]_{LS}$, $K_2 = [CYP{\cdot}L]_{HS}/[CYP{\cdot}L]_{LS}$, and $K_3 = [CYP{\cdot}L{\cdot}L]_{HS}/[CYP{\cdot}L{\cdot}L]_{LS}$.

coordinate high spin heme. In optical difference spectra of [CYP + L] − [CYP], where L is ligand, this leads to a type I spectral change wherein the absorbance at ∼390 nm increases at the expense of the absorbance at ∼420 nm (*11*). For bacterial CYPs such as $P450_{cam}$, the conversion to high spin heme correlates with an increase in the heme redox potential, facilitating the reduction and progression through the catalytic cycle (*12*). The functional effects of spin state change on the reduction potential of and substrate turnover by the mammalian CYPs is not as clear as those with bacterial CYPs (*13*, *14*). However, even if the redox potential were unaffected by the spin state conversion, the displacement of water alone would have significant effects on the rates of the catalytic steps and the uncoupling reactions. Thus, the ligand-dependent spin state change is likely to have important functional consequences in mammalian CYPs, even if the high spin form is not an absolute requirement for metabolism.

The traditional method for monitoring ligand binding based on optical difference spectroscopy is reliable when a single ligand binds. However, when multiple ligands bind simultaneously to a single active site, this method is complicated by several factors. When multiple ligands bind, the extinction coefficients of the high spin states, $[CYP{\cdot}L]_{HS}$ and $[CYP{\cdot}L{\cdot}L]_{HS}$, are not necessarily identical nor are the extinction coefficients of the low spin states, $[CYP{\cdot}L]_{LS}$ and $[CYP{\cdot}L{\cdot}L]_{LS}$. Furthermore, the equilibrium constants for the conversion between low and high spin states may not be the same for [CYP·L] and [CYP·L·L]. That is, if [CYP·L] could be isolated, then $[CYP{\cdot}L]_{LS} \leftrightarrow [CYP{\cdot}L]_{HS}$ could have a different equilibrium constant than $[CYP{\cdot}L{\cdot}L]_{LS} \leftrightarrow [CYP{\cdot}L{\cdot}L]_{HS}$. The relevant states are detailed in Scheme 1. Each of the ligand states is associated with its own spin state equilibrium. As a result of these complexities, the fractional change in absorbance (e.g., $A_{390} - A_{418}$) does not necessarily report directly on the fractional change of ligand binding in a titration performed according to the traditional protocols (*11*), when multiple ligands bind. The distinction between fractional ligand binding per se and percent spin state conversion when multiple ligands bind has been appreciated previously (*15*, *16*), but no quantitative study of the relevant free energy linkages has addressed these aspects of multiple ligand binding to CYPs. One obstacle to a quantitative understanding of these linked equilibria is the difficulty in isolating and characterizing states of single occupancy, [CYP·L], in the absence of double occupancy states, [CYP·L·L].

Here, we compare the ligand-dependent spin state equilibrium for testosterone (TST) complexation with CYP3A4 by EPR and optical titrations at two different protein concentration realms with respect to K_D (i.e., [CYP3A4] < K_D and [CYP3A4] > K_D). The case where [CYP3A4] > K_D could allow for quantitation and characterization of the single occupancy state [CYP·L] in the absence of significant [CYP·L·L]. Testosterone has previously been shown to yield homotropic cooperativity in both steady-state turnover and absorbance-based equilibrium binding experiments (*6*, *17*, *18*). With these combined approaches of EPR and absorbance spectroscopy, it is possible to construct an approximate free energy landscape for multiple ligand binding. The results indicate that CYP3A4 binds the first equivalent of TST with a higher affinity than the second equivalent, even though the second TST molecule drives the heme more efficiently to the high spin state. Thus, $K_{D_2} > K_{D_1}$, but there is positive cooperativity with respect to the dependence of ligand concentration on the spin state equilibrium. The functional and catalytic implications of these results are discussed.

MATERIALS AND METHODS

Protein Expression and Purification. CYP3A4 NF14 construct was purified and expressed from *Escherichia coli* as described in ref *19*. The purity was >95% by SDS−PAGE analysis. The CYP3A4 concentration (CO and $Fe^{2+}-Fe^{2+}$) was determined by using the ϵ_{450} of 91 mM^{-1} cm^{-1} (*20*). The P450 concentration was determined to be >99% with respect to the P420-associated absorbance peak. CYP3A4 was stored in 100 mM phosphate (pH 7.4) with 20% glycerol at −80 °C.

Absorbance Spectroscopy. The absorbance experiments with CYP3A4 were performed using a Cary 3E absorbance spectrophotometer (Varian Scientific Instruments, Inc., Lake Forest, CA) or an Olis Modernized Aminco DW-2 (Olis, Inc., Bogart, GA) as previously described (*11*, *20*, *21*). Temperature was controlled using a Julabo F30-C compact refrigerated circulator and measured using an external Julabo PT100 temperature sensor (Julabo USA, inc., Allentown, PA). CYP3A4 samples were prepared in 100 mM phosphate (pH 7.4) with and without 20% glycerol. Absorbance spectra were deconvoluted into their high and low spin components, and the broad δ-band using the multiple peak fitting package of Igor Pro 5.0 (Wavemetrics, Inc., Lake Oswego, Oregon) in a similar fashion as described for $P450_{cam}$ (*22*). The relative areas under these peaks were calculated and compared to the low spin reference spectra to estimate percentages of high and low spin (described in greater detail in the results section).

It was found that the type of organic solvent used to dissolve TST in the absorbance experiments was critical. Low concentrations (<2% v/v) of acetonitrile, DMSO, ethanol, methanol, and butanol all caused an apparent overall decrease in the molar extinction coefficients of the CYP3A4 absorbance bands (data not shown). Also, additional decreases

and shifts in the low-spin Soret band at ~416 nm were observed in the presence of 0.5% acetonitrile or 1% DMSO and saturating TST (data not shown). Of the solvents examined, we found that the absorbance spectra were least sensitive to short chain alcohols such as ethanol and methanol. However, in the presence of methanol, TST precipitates at a low concentration (i.e., ~200 μM TST), causing an artifactual saturation of binding, which can lead to an underestimation of CYP3A4 absorbance shifts by TST (Figure S1 of the Supporting Information). TST in the presence of ethanol, on the other hand, precipitates at a higher concentration (i.e., ~1 mM TST) than in the presence of methanol, allowing a larger concentration range to be probed. In addition, ethanol also binds extremely weakly to CYP3A4 with an estimated dissociation constant of ~10 M or ~30% ethanol (Figure S2 of the Supporting Information). Therefore, these absorbance spectra were collected at 1% ethanol, which allowed TST concentrations in the 1 mM range to be attained while keeping the effects of the solvent constant.

Optical Analysis of Spin State Equilibria. The positions of the high and low spin components from the peak fitting (i.e., ~390 and ~420 nm, respectively) permitted analysis of the spin state equilibria. The absorbance amplitude of the low and high spin components should be related to the concentrations of high spin and low spin, respectively, by the Beer−Lambert law (absorbance (A) at their respective wavelengths, path length (b), and extinction coefficient (ϵ)).

$$A_{HS} = A_{390} = \epsilon_{HS} b[HS] \quad (1)$$

$$A_{LS} = A_{420} = \epsilon_{LS} b[LS] \quad (2)$$

The relationship between the concentration of the high spin and the low spin is shown by equilibrium constant between high spin and low spin (K_{spin}), where C is a constant relating the A_{390} and A_{420} to the equilibrium constant.

$$K_{spin} = \frac{[HS]}{[LS]} = \frac{\epsilon_{LS} b A_{390}}{\epsilon_{HS} b A_{420}} = C\frac{A_{390}}{A_{420}} \quad (3)$$

$$C = \frac{\epsilon_{LS} b}{\epsilon_{HS} b} \quad (4)$$

A convenient method to measure a value related to K_{spin} is to normalize the absorbance to the high or low spin component (low spin component at 420 nm in this case) and observe the absorbance of the other component. A value related to ΔK_{spin} can then be determined by subtracting the ΔA_{390}(CYP + L) − ΔA_{390}(CYP).

$$\Delta K_{spin} = \frac{[HS]_{(CYP+L)}}{[LS]_{(CYP+L)}} - \frac{[HS]_{(CYP)}}{[LS]_{(CYP)}} = C\frac{A_{390(CYP+L)}}{A_{420(CYP+L)}} - C'\frac{A_{390(CYP)}}{A_{420(CYP)}} \quad (5)$$

Let us assume that

$$C \approx C' \quad (6)$$

then

$$\Delta K_{spin} = C\left(\frac{A_{390(CYP+L)}}{A_{420(CYP+L)}} - \frac{A_{390(CYP)}}{A_{420(CYP)}}\right) \quad (7)$$

$$A_{420(CYP+L)} = A_{420(CYP)} = 1 \quad \text{by normalization} \quad (8)$$

$$\Delta K_{spin} = C\left(\frac{A_{390(CYP+L)}}{1} - \frac{A_{390(CYP)}}{1}\right) = C(A_{390(CYP+L)} - A_{390(CYP)}) \quad (9)$$

$$\Delta K_{spin} = C\Delta A_{390} \quad (10)$$

This method of analysis has some advantages over methods involving simple absorbance difference, second derivative analysis, curve fitting, or direct measurement of the apparent absorbance bands (*13*, *22*−*25*). First, it is not dependent on knowledge or assumptions of the extinction coefficients as in simple difference spectroscopy, second derivative analysis, or direct measurements of the apparent absorbance spectra (*13*, *23*−*25*). Second, it is sensitive to extremes in K_{spin}, where standard methods might fail. For example, a change from 99% to 99.9% low spin is a 10-fold difference in spin state equilibria, which would register as a 10-fold difference by this method, but it would only measure a 0.1% difference by simple difference absorbance spectroscopy. Third, it is robust method that is insensitive to solvent artifacts or protein concentration. For example, one could compare two different CYP concentrations with similar ligand concentrations and get the same result, assuming the [CYP] ≪ K_S and the ligand concentration is known. Finally, it is more convenient than curve-fitting analysis (*22* and this study), since high and low spin references and special software are not required.

However, there are a couple of disadvantages of this method. First, the potential differences in spectral line widths are not taken into account as with curve-fitting analysis (*22* and this study). Second, the extinction coefficients of the high and low spin Soret bands between [CYP] and [CYP] + ligand (i.e., [CYP·L] or [CYP·L·L]) are presumed to be constant. However, these disadvantages are found in all of the standard methods (*13*, *23*−*25*).

EPR Spectroscopy. Electron paramagnetic resonance (EPR) spectroscopy was performed on a Bruker EMX x-band (Bruker-Biospin, Billerica, MA) EPR spectrometer in liquid nitrogen (77 K), using a liquid nitrogen Dewar insert (Wilmad-Labglass, Buena, NJ) or a Bruker B-VT2000 Eurotherm variable temperature controller with a quartz flow through cryostat (Bruker-Biospin, Billerica, MA). The EPR samples were prepared in 100 mM phosphate with 20% glycerol as a cryoprotectant (pH 7.4). TST in ethanol was titrated into 180 μM CYP3A4, and the final concentration of ethanol was kept <2%. Equilibration between TST and the 180 μM CYP3A4 allows TST to remain bound to protein and not precipitate until 2 mM TST is exceeded. This allows a higher concentration of enzyme to be attained for EPR

than is possible for absorbance experiments. The low spin EPR signal was measured by a double integration method as described in ref *26*. The EPR parameters are shown in the figure legends and were obtained under conditions of nonsaturating microwave power.

Simulations and Curve Fitting of the EPR and Absorbance Equilibrium Titrations. The simulations of the EPR and the absorbance equilibrium titrations were fit against two binding mechanisms:

(1) sequential, ordered binding mechanism:

$$\mathrm{CYP} \overset{K_S}{\rightleftharpoons} \mathrm{CYP{\cdot}L} \overset{\alpha K_S}{\rightleftharpoons} \mathrm{CYP{\cdot}L{\cdot}L}$$

$$\mathrm{CYP} \underset{k_{-1}}{\overset{k_1}{\rightleftharpoons}} \mathrm{CYP{\cdot}L} \underset{k_{-2}}{\overset{k_2}{\rightleftharpoons}} \mathrm{CYP{\cdot}L{\cdot}L}$$

(2) sequential, random binding mechanism

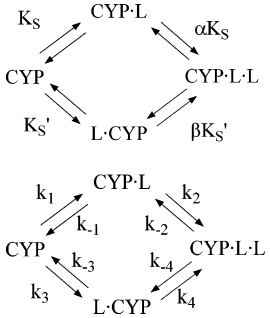

$$K_S = \frac{k_{-1}}{k_1} \tag{11}$$

$$\alpha K_S = \frac{k_{-2}}{k_2} \tag{12}$$

$$K_S' = \frac{k_{-3}}{k_3} \tag{13}$$

$$\beta K_S' = \frac{k_{-4}}{k_4} \tag{14}$$

According to each of these mechanisms, the changes induced by the ligand, TST, on the CYP3A4 EPR and absorbance spectra are dependent on some fractional combination of [CYP·L] and [CYP·L·L].

The spectral changes observed in the TST absorbance titrations were analyzed by Hill plot analysis and fit to eqs 15 and 16 for sequential, ordered binding and eqs 17 and 18 for the sequential, random binding mechanisms that are based on the Adair−Pauling model of allosteric enzymes (*27*):

(1) sequential, ordered binding mechanism

$$[\mathrm{CYP{\cdot}L}] + [\mathrm{CYP{\cdot}L{\cdot}L}] = \frac{[\mathrm{CYP}]_T\left(\frac{[L]}{K_S} + \frac{[L]^2}{\alpha K_S^{\,2}}\right)}{1 + \frac{[L]}{K_S} + \frac{[L]^2}{\alpha K_S^{\,2}}} \tag{15}$$

$$[\mathrm{CYP{\cdot}L{\cdot}L}] = \frac{[\mathrm{CYP}]_T\left(\frac{[L]^2}{\alpha K_S^{\,2}}\right)}{1 + \frac{[L]}{K_S} + \frac{[L]^2}{\alpha K_S^{\,2}}} \tag{16}$$

(2) sequential, random binding mechanism

$$[\mathrm{CYP{\cdot}L}] + [\mathrm{L{\cdot}CYP}] + [\mathrm{CYP{\cdot}L{\cdot}L}] = \frac{[\mathrm{CYP}]_T\left(\frac{[L]}{K_S} + \frac{[L]}{K_S'} + \frac{[L]^2}{\alpha K_S^{\,2}}\right)}{1 + \frac{[L]}{K_S} + \frac{[L]}{K_S'} + \frac{[L]^2}{\alpha K_S^{\,2}}} \tag{17}$$

$$[\mathrm{CYP{\cdot}L{\cdot}L}] = \frac{[\mathrm{CYP}]_T\left(\frac{[L]^2}{\alpha K_S^{\,2}}\right)}{1 + \frac{[L]}{K_S} + \frac{[L]}{K_S'} + \frac{[L]^2}{\alpha K_S^{\,2}}} \tag{18}$$

Derivations of these equations and the classic Adair−Pauling equation can be found in the appendices A−C of the Supporting Information.

The high concentrations of the EPR samples ([CYP] > K_S) prohibited fitting the data to equilibrium-based equations such as the Adair−Pauling equation. Therefore, simulations on the EPR equilibrium titrations were performed using Visual Basic.NET (Microsoft, Redmond, WA). Below are the rate equations used to determine the time-dependent concentrations of [CYP], [CYP·L], [CYP·L·L], and [L] based on the sequential, ordered and random binding mechanisms:

(1) sequential, ordered binding mechanism

$$\frac{\partial[\mathrm{CYP}]}{\partial t} = k_{-1}[\mathrm{CYP{\cdot}L}] - k_1[\mathrm{CYP}][L] \tag{19}$$

$$\frac{\partial[\mathrm{CYP{\cdot}L}]}{\partial t} = k_1[\mathrm{CYP}][L] + k_{-2}[\mathrm{CYP{\cdot}L{\cdot}L}] - k_{-1}[\mathrm{CYP{\cdot}L}] - k_2[\mathrm{CYP{\cdot}L}][L] \tag{20}$$

$$\frac{\partial[\mathrm{CYP{\cdot}L{\cdot}L}]}{\partial t} = k_2[\mathrm{CYP{\cdot}L}] - k_{-2}[\mathrm{CYP{\cdot}L{\cdot}L}] \tag{21}$$

$$\frac{\partial[L]}{\partial t} = k_{-1}[\mathrm{CYP{\cdot}L}] + k_{-2}[\mathrm{CYP{\cdot}L{\cdot}L}] - k_1[\mathrm{CYP}][L] - k_2[\mathrm{CYP{\cdot}L}][L] \tag{22}$$

(2) sequential, random binding mechanism

$$\frac{\partial[\mathrm{CYP}]}{\partial t} = k_{-1}[\mathrm{CYP{\cdot}L}] + k_{-3}[\mathrm{L{\cdot}CYP}] - k_1[\mathrm{CYP}][\mathrm{L}] - k_3[\mathrm{CYP}][\mathrm{L}] \quad (23)$$

$$\frac{\partial[\mathrm{CYP{\cdot}L}]}{\partial t} = k_1[\mathrm{CYP}][\mathrm{L}] + k_{-2}[\mathrm{CYP{\cdot}L{\cdot}L}] - k_{-1}[\mathrm{CYP{\cdot}L}] - k_2[\mathrm{CYP{\cdot}L}][\mathrm{L}] \quad (24)$$

$$\frac{\partial[\mathrm{L{\cdot}CYP}]}{\partial t} = k_3[\mathrm{CYP}][\mathrm{L}] + k_{-4}[\mathrm{CYP{\cdot}L{\cdot}L}] - k_{-3}[\mathrm{L{\cdot}CYP}] - k_4[\mathrm{L{\cdot}CYP}][\mathrm{L}] \quad (25)$$

$$\frac{\partial[\mathrm{CYP{\cdot}L{\cdot}L}]}{\partial t} = k_2[\mathrm{CYP{\cdot}L}] - k_{-2}[\mathrm{CYP{\cdot}L{\cdot}L}] + k_4[\mathrm{CYP{\cdot}L}] - k_{-4}[\mathrm{CYP{\cdot}L{\cdot}L}] \quad (26)$$

$$\frac{\partial[\mathrm{L}]}{\partial t} = k_{-1}[\mathrm{CYP{\cdot}L}] + k_{-3}[\mathrm{L{\cdot}CYP}] + k_{-2}[\mathrm{CYP{\cdot}L{\cdot}L}] + k_{-4}[\mathrm{CYP{\cdot}L{\cdot}L}] - k_1[\mathrm{CYP}][\mathrm{L}] - k_3[\mathrm{CYP}][\mathrm{L}] - k_2[\mathrm{CYP{\cdot}L}][\mathrm{L}] - k_4[\mathrm{L{\cdot}CYP}][\mathrm{L}] \quad (27)$$

Estimates of the concentration of [CYP], [CYP·L], [CYP·L·L], and [L] at equilibrium were estimated by their steady-state concentration at a given TST concentration.

RESULTS

EPR of CYP3A4 in the Presence of Testosterone. Essentially all ligand equilibrium titrations of CYP3A4 reported in the literature have been performed at CYP3A4 concentrations near or below the K_D for binding. Concentrations of [CYP] < K_D are required to extract accurate K_D values, and this provides the rationale for low protein concentration in most experiments. However, experiments performed at much higher protein concentrations ([CYP] > K_D) can uniquely provide information relevant to different binding states such as single occupancy [CYP·L] vs double occupancy [CYP·L·L] states, except in instances of extreme positive cooperativity. EPR is an excellent method for monitoring spin state changes in CYPs, and because it requires high concentrations of protein, it provides a useful probe for the case of [CYP] > K_D. The K_S for TST binding to CYP3A4 determined by difference absorbance spectroscopy has been reported to be 41−78 μM (*18*, *28*). Based on this affinity range, we would not expect the EPR experiments with 180 μM CYP3A4 to yield accurate K_D values with standard curve-fitting equations. On the other hand, an advantage of the EPR experimental design is that the high CYP3A4 concentration equilibrates with TST so that high TST concentrations remain in solution and bound to the protein.

Figure 1 shows the effect of TST on the low spin EPR transitions of CYP3A4. As previously shown by others, the high spin heme signals were too weak to be reliably observed at this temperature (77 K) (*26*, *29*, *30*). In the absence of TST (Figure 1A), CYP3A4 shows three low spin EPR transitions, $g_z = 2.41$, $g_y = 2.23$, and $g_x = 1.87$. In the presence of 1 molar equivalent of TST (i.e., 180 μM), no significant shifts or changes in the line shape of the EPR transitions and only a small decrease in the amplitude of the EPR transitions (Figure 1A) were observed. This small effect on the EPR signal amplitude is consistent with [CYP3A4·TST] complex formation, which is expected at 180 μM TST. Therefore, the first equivalent of bound TST does not have a significant effect on spin state equilibria. At near saturating TST (~2 mM), the amplitudes of the low spin CYP3A4 EPR transitions decrease significantly and the g_z transition is shifted to 2.43, consistent with conversion to the high spin state. This suggests that it is the second equivalent of TST and not the first that induces the low to high spin state conversion.

To understand quantitatively the degree of spin state conversion, the low spin EPR spectrum was examined in the presence of aniline (Figure 1B). Aniline is a well-known type II binder to CYP3A4, shifting the equilibrium nearly completely to the low spin state. Aniline thus provides a quantitative benchmark for the spectral intensity of ~100% low spin state for CYP3A4 (*31*, *32*). With aniline bound, the EPR spectrum was double integrated to estimate the relative concentration of the low spin state in the various stages of the CYP3A4 titration with TST (*26*). It should be noted that the intensity measured by the double integration method is relatively insensitive to the active site environment and provides direct quantitation of the relative spin concentration. This method of quantitation can be contrasted to the method of quantitation reliant on molar extinction coefficients used in optical spectroscopy. In optical spectroscopy, the extinction coefficient of the low spin state or the high spin state may depend highly on the nature of the ligand bound and the active site environment. As a result, the absorbance intensity at any wavelength can only be related to concentration if the extinction coefficient is accurately known. With the EPR method of double integration, the double integrated amplitude is, in many cases, a direct measurement of the concentration of the specific spin system, that is, the low spin state of CYP3A4, under the specific instrumental conditions used (*26*). Thus, from a reference of known spin state, the relative EPR integrated intensity yields relative concentration.

The EPR transition amplitudes of the [CYP3A4·aniline] complex were larger than the low spin EPR signal of CYP3A4 without ligands, which is consistent with absorbance measurements of aniline (*31*) and other type II ligands (*25*). The EPR transitions of the low spin signal of CYP3A4 were $g_z = 2.43$, $g_y = 2.23$, and $g_x = 1.88$, numbers consistent with previous results from rat liver microsomes (*31*). Because the experiments were performed with saturating aniline (~22 mM), we assume that the percent of low spin population was ~100%, which is consistent with the spectral analysis of the Soret absorbance bands (see next section). Figure 1C shows the double integral of the aniline-induced (dashed line) and TST-induced (solid lines) low spin EPR spectra at multiple TST concentrations.

Considering first the spectrum with no TST present (Figure 1A) and assuming that aniline yields 100% low spin CYP3A4, the double integral of the EPR spectrum in the absence of ligands can be divided by the double integral intensity in the presence of aniline, providing the percentage of low spin and high spin and K_{spin} (eq 15). Based on this, the relative concentration of low and high spin and the K_{spin}

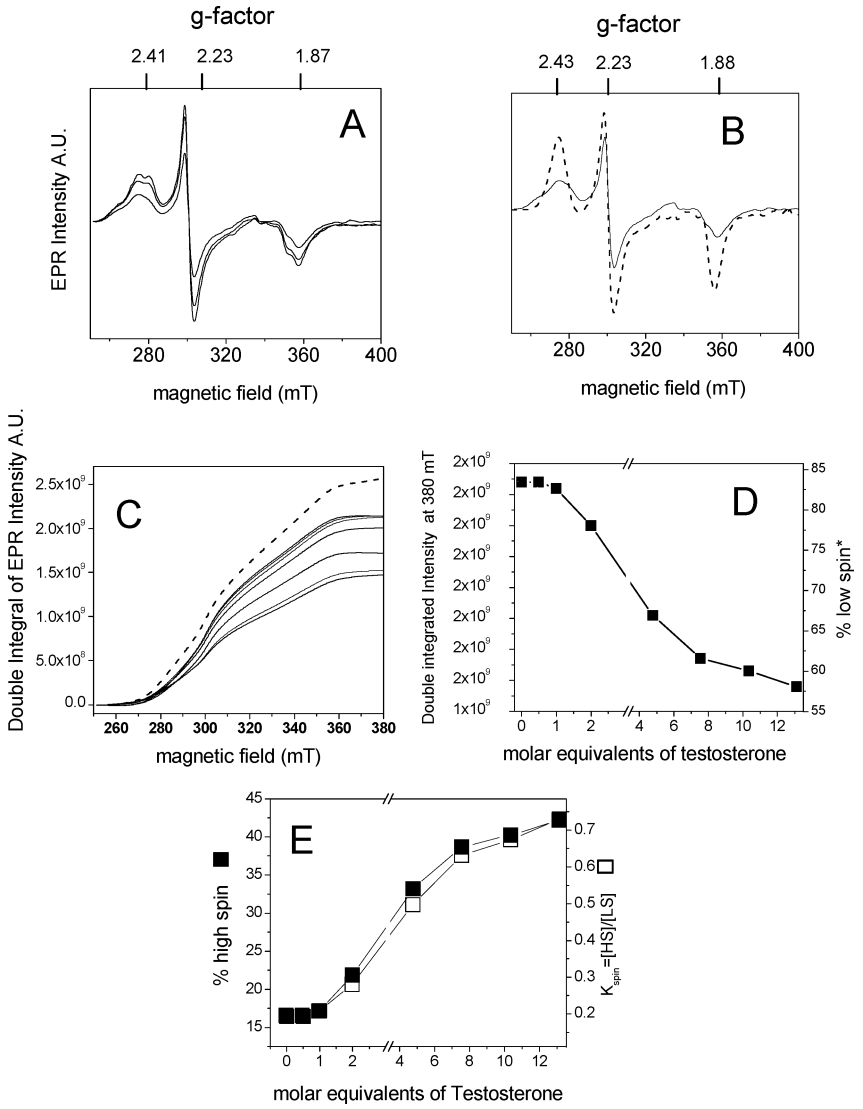

FIGURE 1: Estimation of relative low spin concentration of CYP3A4 by EPR spectroscopy at −196 °C: (A) low spin EPR spectra of 180 μM CYP3A4 in the presence of no TST, 1 equiv of TST, and saturating TST (i.e., 2.3 mM); (B) low spin EPR spectra of 180 μM CYP3A4 in the presence of 22 mM aniline and 2.3 mM TST; (C) double integrals of 180 μM CYP3A4 with 22 mM aniline (− − −) and a variety of TST concentrations (—); (D) amplitude of the double integral at 380 mT and the relative low spin concentration as a function of molar equivalents of testosterone with the calculated low spin percentage on the right axis; (E) calculated percentage of high spin (100% − percentage of low spin, ■) and the K_{spin} (% high spin/% low spin, □). EPR parameters are as follows: temperature = 77 K; modulation amplitude = 16 G; microwave frequency = 9.41276 GHz; microwave power = 6.32 mW; conversion time = 1310.72 ms; time constant = 81.92 ms. Percentage of low spin was estimated by dividing the double integrated EPR intensities at 380 mT of CYP3A4 in the TST titration by the value determined for CYP3A4 with 22 mM aniline, which is ∼100% low spin.

of CYP3A4 were determined to be 84%, 16%, and 0.19, respectively, in the ligand free state. A plot of the amplitude of the double integral of the low spin EPR spectra at 380 mT vs [TST] is shown in Figure 1D with the low spin concentration shown on the right axis. The calculated concentrations of high spin (left axis) and K_{spin} (right axis) are shown in Figure 1E. Increases in TST concentration led to small changes in the spin state until [TST] > 1 molar equivalent, which was evident as a lag phase. At [TST] > 1 molar equivalent, the low spin EPR signal decreased in intensity. As saturation was approached (i.e., [TST] = 1 mM), the amplitude of the low spin CYP3A4 EPR transitions decreased significantly, and the g_z transition was shifted to g_z = 2.43. The decrease in the EPR amplitudes in the presence of near saturating TST is consistent with the conversion of low spin heme iron to high spin heme iron, as was observed previously in EPR studies with steroid−CYP complexes (e.g., ref *33*). After 1 equiv of TST was added, the decrease in spin concentration appeared approximately hyperbolic in shape with an asymptote at ∼50% low spin (i.e., ∼50% high spin and K_{spin} = 1), indicating that the CYP3A4 was only partially shifted to the high spin state. This behavior is consistent with the observation by EPR and absorbance that saturating concentrations of type I ligands sometimes afford a mixture of high and low spin states (*11*, *34*).

Taken together, the lag phase in the EPR experiments demonstrates that the first molecule of TST bound to CYP3A4 does not induce a transition to the high spin state, but binding of the second TST does. EPR experiments also demonstrate that TST does not convert CYP3A4 to 100% high spin, but CYP3A4 remains 50% low spin at saturating TST. This second point is considered further below.

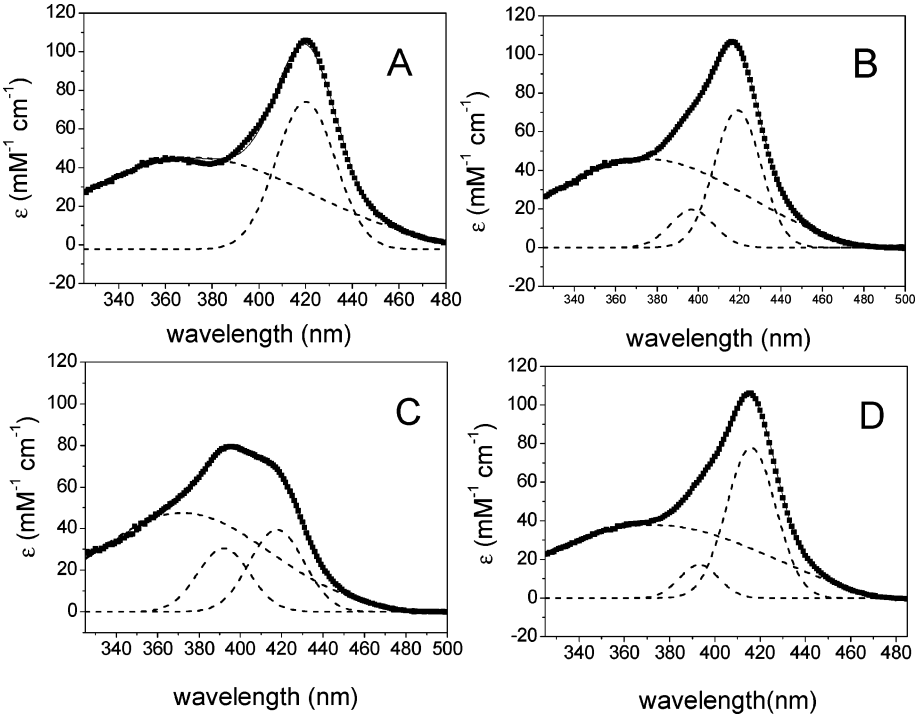

FIGURE 2: Estimation of relative low spin and high spin concentrations of CYP3A4 by absorbance spectroscopy at 25 and 1 °C. The δ-band, low spin, and high spin associated Soret absorbances of 0.65 μM CYP3A4 were fit with Gaussian curves (− − −) in the presence of (A) 22 mM aniline, (B) no TST, (C) 1.28 mM TST, and (D) no TST at 1 °C. The sum of these Gaussian curves is shown as a solid line under the points. All samples contained 1% ethanol.

The spin state equilibria of CYPs in the liquid state has been shown to have some temperature dependence (*23*, *35*−*37*). These temperature effects on the spin state equilibria could also manifest themselves in the solid state, so the EPR experiments were repeated at a variety of temperatures (i.e., 77 K (−196 °C) to 230 K (−40 °C)). This change in temperature was found to not significantly alter the high and low spin equilibria within the level of the noise (data not shown). This is consistent with absorbance spectroscopy of partially purified bovine CYP at 77 and 293 K, which demonstrated only small changes of the spin state related absorbance peaks as a function of temperature (*33*). It is also consistent with the shifts induced in the absorbance peaks at 1 and 25 °C in isolated CYP3A4 (see below). In summary, temperature does not significantly affect K_{spin} under the conditions and temperature ranges used here.

Estimates of the Relative Percentages of High and Low Spin States by Absorbance Spectroscopy. The EPR results indicate that saturating concentrations of TST are insufficient to generate a dominant high spin state. To examine more closely the optical effects of TST on CYP3A4 and to validate the incomplete conversion to the high spin state by TST, the Soret region of the CYP3A4 spectrum was monitored in the absence of TST and in the presence of near saturating TST concentrations. The spectra were modeled with a peak-fitting analysis to approximate the individual components contributing to the spectra as described previously on $P450_{cam}$ (*22*).

Figure 2 shows the optical absorbance spectra along with their deconvolution into a three-component Gaussian model. This model includes a low spin component (∼416−420 nm), a high spin component (∼390−405 nm), and a shoulder centered at ∼360 nm that is always observed in CYP absolute spectra (e.g., ref *25*). These peaks correspond to the low-spin associated Soret, high-spin associated Soret, and δ-bands, respectively (*25*). There are no ligand-specific spectral effects on the δ-band reported in the literature, unlike the classic effects on the low spin and high spin components. At ∼416 nm, in the absence of ligands, there is a peak that typically shifts to a longer wavelength (e.g., 420 nm) in the presence of type II ligands such as aniline (*38*, *39*). On the other hand, binding of type I ligands induces a decrease in the low spin associated Soret peak with a concomitant increase in a peak at shorter frequency, implying that it is associated with the high-spin state (*11*).

Figure 2A shows the deconvolution of the absorbance spectrum of CYP3A4 with 22 mM aniline. The direct absorbance spectrum can be deconvoluted into two components, including a δ-band and a low spin component centered at 372 and 420 nm, respectively. This fit is consistent with our previous assertion that CYP3A4 is ∼100% low spin in the presence of saturating aniline and justifies our use of CYP3A4 with saturating aniline as a low spin reference. The fitted low spin Soret peak in this aniline sample was found to have an $\epsilon_{420} = 76.5$ mM^{-1} cm^{-1} and a line width of 14.1 nm.

Figure 2B shows the deconvolution of the absorbance spectrum of CYP3A4 without ligands. There is a low spin absorbance peak centered at ∼416 nm and a high spin peak centered at ∼393 nm, which can be deconvoluted into a δ-band and a high and a low spin component centered at 375, 396, and 419 nm, respectively. The relative area of the low spin component was ∼83% with respect to the low spin reference, giving a high spin value of 17% and a $K_{spin} = K_1 = 0.20$. This is in range of the value obtained by Davydov and co-workers of 19% ± 4% (*40*). This is also close to the results obtained by EPR, which showed that the high spin and low spin complexes contribute 16% and 84%, respec-

tively. However, it should be noted that comparisons between absorbance and EPR spectroscopy should be treated cautiously because there are small errors in both experimental measurements and there is a small but significant entropic component (see below). These results are consistent with the mixed spin state observed previously by EPR spectroscopy with rabbit liver microsomes (*29*).

Figure 2C shows the deconvolution of the absorbance spectrum in the presence of near saturating TST. Higher TST concentrations were not obtainable in the absorbance experiments due to ligand precipitation. The high spin associated Soret peak increases significantly in intensity, whereas the low spin state associated Soret peak decreases in intensity, which is consistent with a transition to the high spin state. This can be deconvoluted into a δ-band and high and low spin components centered at 372, 392, and 418 nm, respectively. The relative area of the low spin component is 46% with respect to the low spin reference, giving a high spin concentration of 54% and a $K_{spin} = K_3 = \sim 1.17$. The K_3 value obtained from this measurement should be considered approximate because the concentration of TST is not completely saturating. The integrated areas under each of the components are in good agreement with our EPR experiments at high TST concentration, where low spin was ~50%.

Figure 2D shows the deconvolution of the absorbance spectrum in the absence of ligands at 1 °C. Again, this was deconvoluted into a δ-band and high and low spin components centered at 373, 393, and 416 nm, respectively. There was a notable increase in the percentage of low spin and a decrease in the percentage of high spin with a decrease in temperature, which has been observed previously in a variety of CYPs, including CYP3A4 (*23*, *35*−*37*). The integrated area is 7% greater than CYP3A4 without ligands (Figure 2B), implying a 7% decrease in percentage of high spin. This is consistent with the 4.1% decrease in high spin observed in partially purified rat CYP between 4 and 20 °C (*35*) or the small change in absorbance amplitude observed for partially purified bovine CYP between 25 and −196 °C. The temperature-induced changes in spin state equilibria in isolated CYPs (*33*, *35*) are considerably less sensitive to temperature than microsomal preparations, implying a lipid phase transition in the microsomal preparations (*23*, *35*, *36*). The temperature dependence of TST binding was also weakly temperature-sensitive (data not shown), which is consistent with the weak temperature sensitivity observed for several substrates of $P450_{cam}$ (*37*).

In addition, some error in the absorbance method is expected because the extinction coefficients in the presence of ligand (i.e., TST) are likely to differ considerably from those used for spectral models (i.e., SDS or aniline). In fact, it has been shown previously that the extinction coefficients of CYP absorbance bands can be significantly affected by ligands (*25*). Regardless of the uncertainties associated with deconvolution of optical spectra, our results suggest that even at saturating TST, CYP3A4 is only partially (~50%) high spin. This result is consistent with EPR of type I ligands (*11*, *34*) and second derivative analysis of rat CYP with TST, where only 33% was estimated to be high spin at 500 μM testosterone (*13*).

Normalized Absorbance Spectra Demonstrate That Spin State Equilibrium Is Positively Cooperative with Respect to Testosterone Binding. As shown in the model spectra discussed above, low and high spin states have significant spectral overlap in the region 390−420 nm. This makes difficult an analysis of the low spin state alone. However, the models suggest that at wavelengths below 390 nm changes in absorbance would directly affect changes in the percentage of K_{spin} as described in the Materials and Methods. Therefore, the spectra were normalized at 420 nm and monitored for ligand-dependent increases in absorbance at 390 nm. Absolute spectra and difference spectra, normalized at 420 nm, are shown in Figure 3, panels A and B, respectively. When the amplitude of the absorbance difference at 390 nm is plotted, an apparent sigmoidal increase is observed, including an associated lag phase, in advance of the TST-induced high spin state (Figure 3C). From this trace and a Hill analysis, we obtained values for the $K_S = 200$ μM and $n = 1.30$ (Figure 3C, inset). These values are consistent with the positive cooperativity ($n > 1$) observed previously (*18*, *28*). However, this value differs considerably from the K_S values obtained previously ($K_S = 41-78$ μM) (*17*, *18*, *28*), which were performed with TST dissolved in methanol rather than ethanol. In our hands, TST titrations of CYP3A4 done with methanol instead of ethanol as a ligand solvent precipitated at a lower concentrations of TST than those in ethanol, leading to lower estimates of K_S (Figure S1 of Supporting Information).

Within the context of the sequential, ordered binding model, two extreme cases are considered. In the first case (case 1), [CYP3A4·TST·TST] and [CYP3A4·TST] both contribute equally to the transition to high spin state as described by eq 15. In the second case (case 2), the first ligand binding event is spin state "silent" with a [CYP·TST] and only [CYP·TST·TST] contributes to the transition to high spin state as described by eq 16. Thus, the concentration of high spin complex would be directly proportional to [CYP·TST·TST] concentration.

The equilibrium binding data were fit to both Adair−Pauling eqs 15 and 16, and the quality of fits was compared. From these analyses, α, K_S, and αK_S values for each of the curves described by either eq 15 (i.e., case 1) or eq 16 (i.e., case 2) were obtained. In case 1, curve fitting of Figure 3C by eq 15 (dashed line) produced values of $\alpha = 0.14$, $K_S = 716$ μM, and $\alpha K_S = 100$ μM with the second binding event displaying higher affinity than the first (i.e., $K_S > \alpha K_S$). In case 2, curve fitting of Figure 3C by eq 16 (solid line) produced values of $\alpha = 20$, $K_S = 22$ μM, and $\alpha K_S = 440$ μM with the first binding event displaying higher affinity than the second (i.e., $K_S < \alpha K_S$).

The Curve-Fitting Results Are a Conundrum Because Both Models Are Described Well by the Data. In case 1, a lag phase or sigmoidal shape is observed, because the $\alpha K_S < K_S$ induces an increase in the spectral slope (i.e., δ(absorbance)/δ[TST]) at increasing TST concentration. This increase in spectral slope arises because formation of [CYP3A4·TST] produces a population of higher affinity sites for the second TST binding. For case 2, involving $\alpha K_S > K_S$, a lag is also observed because only the [CYP·TST·TST] and not [CYP3A4·TST] elicits a transition to the high spin state. Here, no significant increase in the high spin fraction is observed until the first site, [CYP3A4·TST], is nearly saturated. This is a dramatic reminder that curve-fitting alone

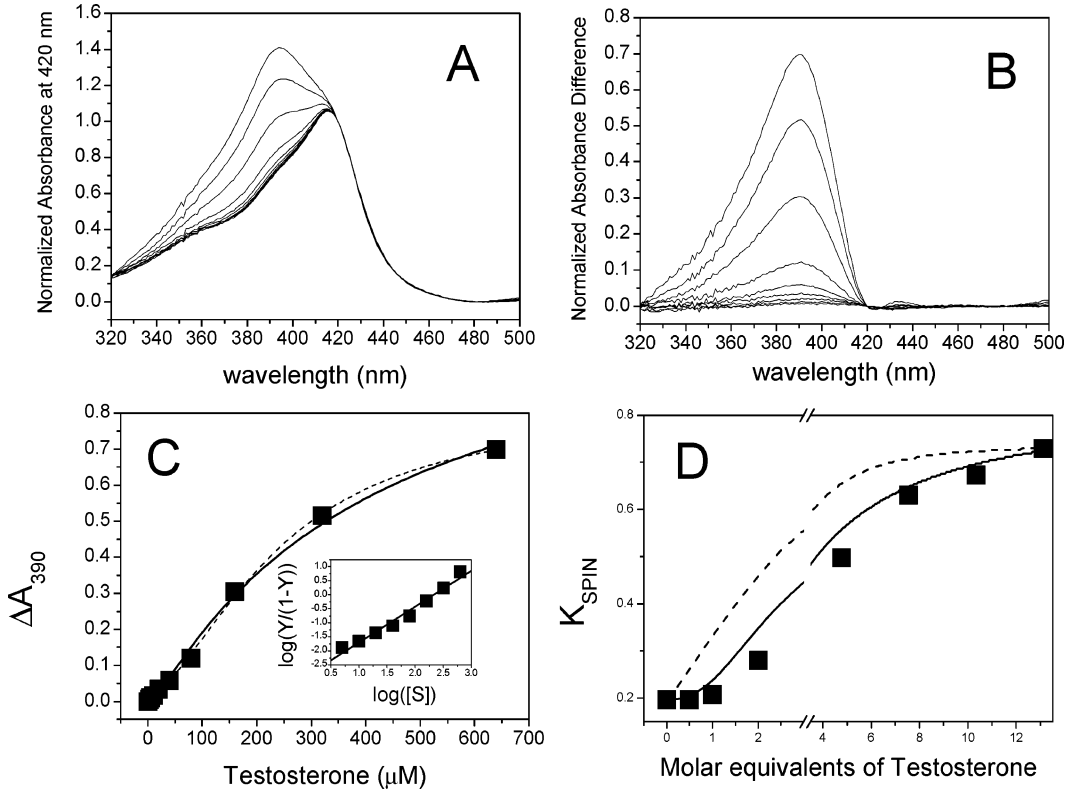

FIGURE 3: Optical analysis of spin state equilibrium (K_{spin}) by normalized difference absorbance spectroscopy at 25 °C*:* (A) absolute absorbance spectra of the 1.3 μM CYP3A4 at various TST concentrations normalized on 420 nm; (B) CYP3A4 with TST at various concentrations minus CYP3A4 without TST normalized at 420 nm; (C) amplitude of the 390 nm peak in Figure 3B as a function of testosterone concentration with Adair−Pauling equation fits of the sequential, ordered binding model (—, − − −) and Hill plot analysis (inset), where *Y* represents the fractional increase of absorbance at 390 nm; (D) calculated K_{spin} value of the EPR equilibrium binding titration from Figure 2E fit with simulations based on Adair−Pauling equation fits in panel C (—, − − −).

may be misleading in the absence of a complete analysis with multiple experimental methods.

The EPR experiments performed at [CYP] > K_S provide an opportunity to resolve this conundrum. Thus, the experiments described in Figure 2D are revisited here in Figure 3D. Simulations of the spin state changes at this high protein concentration using values obtained by curve-fitting Figure 3C have been normalized against the calculated K_{spin} values of the EPR equilibrium binding titration curve (cf. Figures 1D and 3D). The simulation of case 1, where both [CYP3A4·TST] and [CYP3A4·TST·TST] contribute equally to the high spin state transition, is shown as a dashed curve in Figure 3D. The simulation of case 2, where only [CYP3A4·TST·TST] induces the transition to high spin state, is shown as a solid curve in Figure 3D. Obviously, the data fit significantly better to the simulation of case 2, although the fit is not perfect because of small temperature differences between the EPR and absorbance spectroscopy (see above). In this simulation, a significant lag phase is observed that is also present in the EPR equilibrium titration whereas the simulation of the case 1 obviously lacks this lag phase. The lag phase is consistent with a nonproductive binding mode, where there is no shift in the spin state equilibrium. Binding of the first ligand is followed by binding of the second, which induces the transition to high spin state. Therefore, the data are most consistent with a reaction coordinate for binding of TST to CYP3A4 that includes $K_{D_2} > K_{D_1}$ with respect to two ligands binding and positive cooperativity with respect to the ligand binding and formation of the high spin state. The relationship between the dissociation constants (i.e., $K_{D_2} > K_{D_1}$) and sigmoidal spectral changes with respect to inhibitor concentration using absorbance and EPR spectroscopy have also been observed in the photosynthetic enzyme cytochrome b_6f complex with the inhibitor 2,5-dibromo-3-methyl-6-isopropylbenzoquinone (DBMIB) (*41*, *42*).

Case 2 presented above may not provide the best fit for two TST binding, so the sequential, random order binding mechanism was also fit to data of Figure 3C, in which all the ligands (eq 17, case 3) or only the last ligand contributes to the conversion to the high spin state (eq 18, case 4). In terms of ligand contributions to the high spin state conversion, case 3 and case 4 can be considered analogous to case 1 and case 2 of the sequential, ordered binding mechanism. The sequential, random order mechanism is equivalent to the "two-site" model that has become commonly used to fit steady-state kinetic data for CYPs. In this model, two nonidentical sites can be independently occupied in either order. This is a more general model than the sequential, ordered mechanism, which requires occupation of one site before the other. The quality of the fit to the random order binding model was examined in Figure 4A, showing that both case 3 (dotted line) and case 4 (solid line) have equivalent fits as case 1 and case 2. Case 3 has $\alpha = 0.014$, $K_S = 2281$ μM, $\alpha K_S = 32$ μM, $\beta = 0.067$, $K_S' = 1044$ μM, and $\beta K_S' = 70$ μM, while case 4 has $\alpha = 14.6$, $K_S = 27.5$ μM, $\alpha K_S = 401.5$ μM, $\beta = 1.17 \times 10^{-5}$, $K_S' = 30\,650$ μM, and $\beta K_S' = 0.36$ μM. The values obtained by fitting Figure 4A with eqs 17 (case 3) and 18 (case 4) were normalized against the calculated K_{spin} values of the EPR equilibrium binding titration of Figure 1E, and this is revisited in Figure

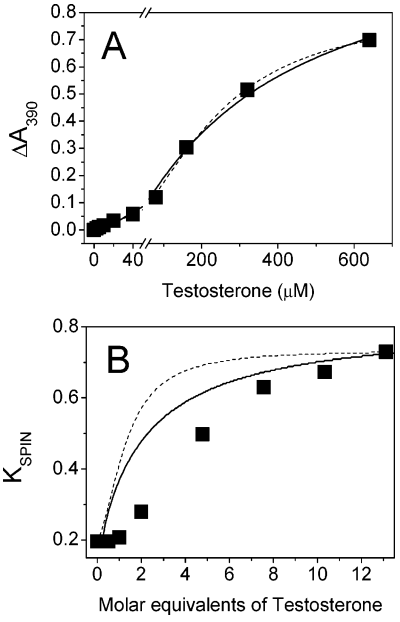

FIGURE 4: Amplitude (A) of the 390 nm peak in Figure 3B as a function of TST concentration with Adair−Pauling equation fits of the sequential, random binding model (—, − − −) and calculated K_{spin} (B) from the EPR equilibrium binding titration from Figure 2 fit with simulations based on Adair−Pauling equation fits in panel A (—, − − −).

4B, where the quality of fits were compared. Both case 3 (Figure 4B, dotted line) and case 4 (Figure 4B, solid line) fit poorly to the data when compared with case 2 (Figure 3D). Importantly, neither of the two-site random order models predicts a lag phase in the spin state shift, but the sequential, ordered models do. Therefore, case 2 is the simplest model that fits the data and will be used as a template for the hypothetical model explained below.

DISCUSSION

CYP3A4 exhibits complex, nonhyperbolic ligand binding behavior and non-Michaelis−Menten steady-state kinetics for some substrates (*4*, *6*, *7*). This implies that cooperativity occurs between multiple events in the complex reaction cycle or in the ligand binding reaction coordinate and that multiple ligands bind simultaneously to a single CYP3A4. However, the extent to which the elementary steps within these complex reactions are cooperative has not been fully elucidated. Historically, optical difference spectroscopy has been used to monitor ligand binding to CYPs, wherein ligands perturb the ferric spin state equilibrium (*11*). However, when multiple ligands bind simultaneously, the simple difference in absorbance (e.g., $A_{390} - A_{418}$) does not reliably report on individual steps that contribute to the overall binding coordinate. This complexity, which has been acknowledged previously (*43*), must be understood to quantitatively assess the partitioning between [CYP], [CYP·L], and [CYP·L·L] at subsaturating concentrations of ligand. Therefore, we revisited the binding of TST to CYP3A4 using a combination of experimental approaches. We exploited conditions of high [protein]/[ligand] to characterize [CYP3A4·L], which induces no apparent perturbations in the spin equilibria in the absence of significant concentrations of the doubly bound state [CYP3A4·L·L]. The fundamentally important conclusions derived directly from experimental observations are that (1) the first equivalent of TST that binds to CYP3A4 causes negligible perturbation of the heme spin state equilibrium, (2) double occupancy states of the CYP3A4/TST equilibria remain significantly low spin, although they do elicit a higher percentage of the high spin state than the single occupancy states, and (3) the first equivalent of TST binds with higher affinity than the second, in contrast to what has been assumed based on previous optical titrations of CYP3A4 with TST.

Because of the sigmoidal nature of the spin state shift versus TST concentration curves, it has been assumed previously that binding of TST is positively cooperative. Our data demonstrate the feasibility of negative cooperativity of binding yielding sigmoidal curves when spin state is plotted against TST concentration, when the second ligand binds more weakly but drives the spin state change. The situation here does not necessarily reflect negative cooperativity according to its strictest definition, wherein binding of the first TST causes some change in the inherent affinity of the second binding site for the second TST. Our data do not address mechanistic aspects of cooperativity of binding according to this definition. In the model that best fits the data, the first TST merely occupies the higher affinity site, resulting in a protein with a lower affinity for the next TST. No direct causal role of the first TST on the affinity of second is required, so negative cooperativity is not strictly operative. However, the fact is that the second TST has a lower affinity than the first and this has the same functional consequences as negative cooperativity in terms of ligand distribution at subsaturating TST concentration. For both "true" negative cooperativity and the sequential, ordered binding mechanism, the lower affinity of the second TST leads to a preference for [CYP3A4·TST] over [CYP3A4·TST·TST] at low TST concentration, and this preference is greater than a simple statistical effect. Thus, TST binding to CYP3A4 behaves functionally as a negatively cooperative binding system and not a positively cooperative one.

The results and conclusions derived from this study allow for a more detailed analysis of linked free energies of ligand binding and ligand-dependent spin state equilibrium, as outlined in detail below (Scheme 2). The results also demonstrate an interesting case in which the binding of ligand to a CYP can occur with $K_{D_2} > K_{D_1}$, whereas the ligand-dependent conversion to the high spin state can be positively cooperative with respect to ligand concentration.

We acknowledge that some experimental data suggest the possibility that three TST molecules bind to each CYP3A4 (*44*, *45*). Although this is an intriguing possibility that demands additional consideration, the analysis below limits the TST stoichiometry to 2:1. None of our spectral data summarized here provide any compelling evidence for a third TST binding event. It is possible that two TST molecules bind with very similar kinetic and energetic behavior and a third TST binds with different behavior, thus affording an apparent "fit" to two binding events. In the absence of additional evidence, however, the simpler model with only two binding events is preferred.

We propose a thermodynamic cycle for TST binding to CYP3A4 as diagrammed in Scheme 2A, which provides a quantitative revision of the generic scheme presented in Scheme 1. The values for the spin equilibria and the dissociation constants determined experimentally are shown in Scheme 2A. To better understand the energetic landscape

Scheme 2: Quantitative Model for the Thermodynamic Linkage between TST-Dependent Ferric Spin State Equilibrium of CYP3A4[a]

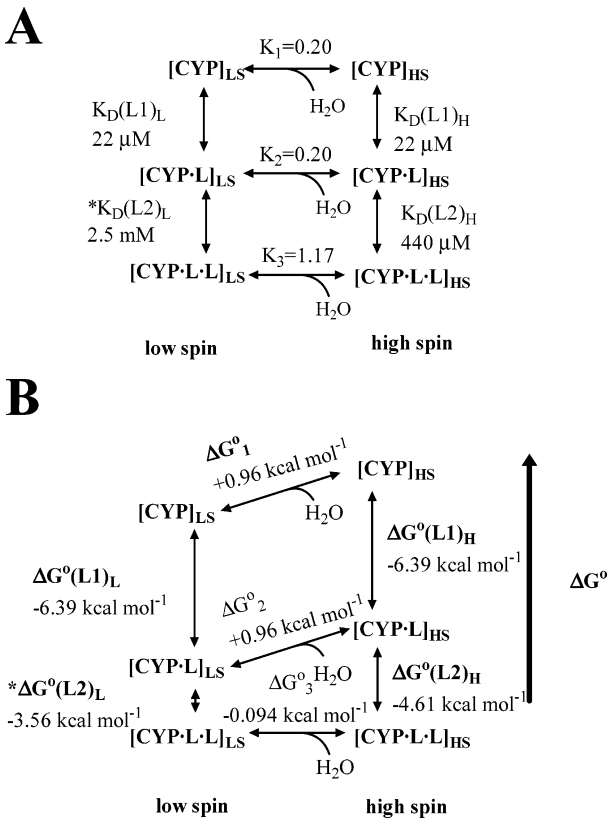

[a] The same abbreviations are used in part A as in Scheme 1. (A) Dissociation constants and equilibrium constants determined experimentally or estimated as they relate to the low and high spin states. (B) Standard free energies (i.e., $\Delta G°$) for the states are shown in part A. Longer vertical arrows represent more favored binding. Positively sloped horizontal lines represent less favored equilibria toward the high spin state. The $\Delta G°(L2)_L$ and $K_D(L2)_L$ were calculated by their thermodynamic relationship.

of TST binding, these values were converted to $\Delta G°$ ($\Delta G° = RT \ln(K_{eq})$, where $R = \sim 2$ cal K^{-1} mol^{-1}, $T = 298$ K, and K_{eq} = equilibrium constant) and are shown diagrammatically in Scheme 2B. The vertical dimension shows increasing free energy toward the top, so energetically favored species are closer to the bottom of the diagram. Also, the lengths of the vertical arrows represent relative free energy changes so that larger ΔG values have longer vertical arrows. In the absence of TST, CYP3A4 is in equilibrium between high and low spin states.

From the values determined by absorbance, we were able to determine the relative concentrations of the high and low spin states and K_1, which were determined to be approximately 17%, 83%, and 0.2, respectively (Figure 2). At a substoichiometric concentration of TST, there is a negligible change in the relative concentration of the high spin state and low spin state, as shown by EPR. Based on the minimal perturbation of the spin state with the first equivalent of TST, this ligand must have similar affinities for the high spin and low spin states due to thermodynamic linkage considerations. From this, we obtain equilibrium constants K_1 and K_2 of 0.20 and the corresponding $\Delta G_1^\circ = \Delta G_2^\circ = +0.96$ kcal mol^{-1} (cf. Scheme 2, parts A and B). Because the first equivalent of TST does not have a significant effect on the spin state equilibrium, we propose that the first TST binds relatively far from the heme. Interestingly, the recently published crystal structure of CYP3A4 with progesterone bound indicates that the ligand binds at a peripheral site >17 Å from the heme iron (*46*). Possibly, steroids such as TST or progesterone bind at such a distal site with higher affinity than the active site, but our experiments provide no structural information.

From the absorbance spectroscopy, we find that the $K_D(L1)_L$ and $K_D(L1)_H$ of TST binding in each of these states is approximately 22 μM (Scheme 2A), corresponding to a $\Delta G°(L1)_L = \Delta G°(L1)_H = -6.39$ kcal mol^{-1} (Scheme 2B). As we increase the concentration of TST, we find a transition from the low spin state to the high spin state. From the absorbance data (Figure 3C), we were able to estimate the dissociation constant, $K_D(L2)_H$ (Scheme 2A), for TST binding to the high spin state of [CYP3A4·TST] to be 440 μM, corresponding to a $\Delta G°(L2)_H = -4.61$ kcal mol^{-1}. On the basis of the absorbance data (Figure 2D), we determined $K_3 = \sim 1.17$ (Scheme 2A) and a $\Delta G_3^\circ = -0.094$ kcal mol^{-1} (Scheme 2B). Using thermodynamic linkage relationships, it is possible to calculate the free energy of testosterone binding to the low spin state. The value is $\Delta G°(L2)_L = -3.56$ kcal mol^{-1} (i.e., $\Delta G_2^\circ + \Delta G°(L2)_H - \Delta G_3^\circ = \Delta G(L2)_L$; 0.96 kcal mol^{-1} + ($-4.61$ kcal mol^{-1}) − (-0.094 kcal mol^{-1}) = -3.56 kcal mol^{-1}), corresponding to a dissociation constant for the second ligand in the low spin state of $K_D(L2)_L = 2.5$ mM (cf. Scheme 2, parts A and B). Thus, we can directly measure or estimate all of the parameters that define the complete thermodynamic linkage between all states in this working model of TST binding. Therefore, while the $K_{D_2} > K_{D_1}$, as indicated by a longer vertical arrows for the first TST vs the second TST, the formation of the high spin state is positively cooperative with respect to TST binding as indicated by horizontal arrow (slope = 0) for ΔG_3° compared to ΔG_1° and ΔG_2°, which both have positive slope (Scheme 2B). We acknowledge that this is a semiquantitative treatment due to the necessary simplifying assumptions that $K_1 = K_2$ and $\Delta G_1^\circ = \Delta G_2^\circ$. We anticipate that K_1 and K_2 are identical only within the limits of the experimental techniques; it is highly unlikely that they are identical in reality.

Working Model for the Relationship between Testosterone Binding to CYP3A4 and Turnover. Regardless of these sources of minor error, we propose that the first tight binding of testosterone occurs in a nonproductive fashion away from the heme, which leads to little change in the spin state. As noted above, this may be related to the peripheral binding site observed in the recently solved crystal structure of progesterone on the CYP3A4 surface (*46*). Regardless, both occupations of a nonproductive cleft in the active site or of a peripheral site by TST have a negligible effect on the spin state equilibrium. The first TST could make binding of the second TST less energetically favorable, explaining the apparent decrease in affinity for the second TST. However, when the second TST does bind, it increases the probability of generating the high spin complex, although it does not completely drive the system to the high spin form. The increases in the high spin fraction upon binding the second TST are, by definition, positive cooperativity between TST binding and high spin complex formation.

The thermodynamic relationship of different binding states of our working model can be conveniently visualized using coupling free energies. The coupling free energy for a series

of linked equilibria is the difference between the sum of the free energies of the individual equilibria for the separate reactions and the actual free energy change in the linked reaction. A negative coupling free energy here is defined as positive cooperativity. For example, in this case the coupling free energy for the binding of the first and second molecules of TST to the CYP3A4 low spin state is $\Delta\Delta G°(L)_{LS} = \Delta G°(L2)_{LS} - \Delta G°(L1)_{LS} = -3.56$ kcal mol^{-1} $-$ (-6.39 kcal mol^{-1}) $= +2.83$ kcal mol^{-1}. This is the difference in free energy of binding for a TST molecule in the presence and absence of another TST. The coupling free energy for TST binding to the high spin state is similarly $\Delta\Delta G°(L)_{HS} = \Delta G°(L2)_{HS} - \Delta G°(L1)_{HS} = -4.61$ kcal mol^{-1} $-$ (-6.39 kcal mol^{-1}) $= +1.78$ kcal mol^{-1}. Thus, the second equivalent of TST binds with less affinity to the low spin state than to the high spin state (i.e., less favored or larger positive coupling free energy for the low spin state).

Additional coupling free energy is possible for the linkage between TST binding and water binding to the ferric heme iron. For example, the coupling free energy for water binding to the high spin ligand-free CYP3A4 is $\Delta\Delta G = \Delta G_1° - \Delta G_2° = 0.96$ kcal mol^{-1} $-$ 0.96 kcal mol^{-1} $= 0$ kcal mol^{-1}. The value of $0 = \Delta\Delta G$ indicates that the binding of water and the first equivalent of TST are not coupled, and the binding of one has no energetic effect on the binding of the other. The coupling free energy for binding of water and TST to the $[CYP{\cdot}L]_{LS}$ is $\Delta\Delta G = \Delta G_2° - \Delta G_3° = 0.96$ kcal mol^{-1} $-$ (-0.094 kcal mol^{-1}) $= +1.054$ kcal mol^{-1}. Thus, the binding of water is $\sim$1 kcal mol^{-1} less energetically favorable when the second equivalent of TST is present compared to when only the first TST is present. The water binding is favored by the binding of the first equivalent of TST and the formation of the high spin state is positively cooperative (i.e., formation of the high spin state is promoted by the second equivalent of TST and not the first).

It is instructive to consider the magnitudes of the coupling free energies in addition to their signs. The coupling free energies calculated here range between 0.0 and $\sim$3 kcal mol^{-1}, which are small free energy differences when considered in the context of common molecular interactions. For example, the energy of a "generic" hydrogen bond in water is typically considered to be 3$-$9 kcal mol^{-1} (*47*). Thus, the coupling free energies that contribute to TST binding and spin state conversion are less than the energy of a single hydrogen bond. However, small energy couplings such as those estimated here are sufficient to significantly change populations of species within a mixture. In fact, coupling free energies measured for other protein$-$ligand systems, including hemoglobin and cytosolic malic enzyme, are typically $<$4 kcal mol^{-1} (*48*, *49*). The important point is that small coupling free energies are sufficient to alter the distribution of ligand states when ligand concentration is subsaturating. The coupling free energies estimated here are clearly sufficient to strongly disfavor binding of the second TST but also to disfavor water binding to the heme once the second TST is bound.

It is also useful to relate the results described here to turnover studies with TST. The S_{50} values determined from turnover vary from 51 to 160 μM ($K_S = S_{50}/\ln 2 = 74-213$ μM) with Hill coefficients that vary between $n = 1.3$ and 1.6 (*3*, *6*, *44*). These results are consistent with the Hill equation analysis that we performed on our normalized absorbance titration (Figure 3C, inset and $K_S = 200$ μM, $n = 1.3$) and qualitatively consistent with previous measurements by optical difference absorbance spectroscopy (*18*, *28*). The similarity between the cooperativity in high spin complex formation and catalysis suggests that the spin state may play a functional role in turnover, at least for this substrate. Moreover, the present results provide a clear explanation for the apparent positive cooperativity of binding reported by others: the TST-dependent spin state shift, which was the basis for the binding experiments, is positively cooperative. However, here we have not used as a starting point the assumption that the percentage change in spin state is equivalent to the fractional TST binding. In the absence of this assumption and with a closer examination of the spin state at single occupancy, our data provide the opposite conclusion concerning TST binding per se: CYP3A4 has a lower affinity for the second equivalent of TST than the first.

We propose that the high affinity site ($K_D = 22$ μM) is a "nonproductive" binding site, where TST is not metabolized. A "nonproductive" binding site could partially explain some of the heterotropic effects observed between TST and other ligands (*6*, *7*, *50*). As an effector, TST has different effects on different substrates, including midazolam, nifedepine, α-NF, and others (*6*$-$*8*, *50*). At low TST concentration, less than $\sim$60 μM, TST actually activates terfenadine metabolism, but it becomes an inhibitor at higher concentration (*8*). TST activates metabolism of midazolam at the 1′-position and inhibits formation of 4-hydroxy-midazolam with apparent half-maximal responses of $\sim$10$-$20 μM and 20 μM, respectively, in human liver microsomes (*8*). In contrast, other CYP3A4 substrates are affected only at relatively high TST concentrations with significant effects on the turnover only occurring at concentrations $>$100 μM TST (*3*). Thus, the heterotropic interaction of TST with ligands such as αNF are consistent with multiple discrete TST binding sites, some of which compete directly with other ligands (*17*, *18*, *44*, *51*).

Finally, it should be stressed that the results described here for TST cannot be generalized to other type I ligands. The free energy profiles of other substrates/CYP3A4 interactions will presumably be different from TST. In fact, our analysis was simplified, fortuitously, by the $K_{D_2} > K_{D_1}$ of binding, which facilitates capturing the [CYP3A4·TST] complex and allows us to differentiate between the binding models, and by the negligible free energy coupling between the first TST binding and the spin state, which allows for simplifying approximations in the calculation of free energies.

SUPPORTING INFORMATION AVAILABLE

Spectral titration data for testosterone dissolved in ethanol versus methanol, which demonstrate a possible source for underestimation of K_d in methanol, spectral effects of ethanol on CYP3A4, and derivations of the modified Adair$-$Pauling equations described in Materials and Methods. This material is available free of charge via the Internet at http://pubs.acs.org.

REFERENCES

1. Guengerich, F. P. (1999) Cytochrome P-450 3A4: regulation and role in drug metabolism, *Annu. Rev. Pharmacol. Toxicol. 39*, 1−17.
2. Shou, M. (2002) Kinetic analysis for multiple substrate interaction at the active site of cytochrome P450, *Methods Enzymol. 357*, 261−276.
3. Kenworthy, K. E., Clarke, S. E., Andrews, J., and Houston, J. B. (2001) Multisite kinetic models for CYP3A4: simultaneous activation and inhibition of diazepam and testosterone metabolism, *Drug Metab. Dispos. 29*, 1644−1651.
4. Hlavica, P., and Lewis, D. F. (2001) Allosteric phenomena in cytochrome P450-catalyzed monooxygenations, *Eur. J. Biochem. 268*, 4817−4832.
5. Tracy, T. S. (2003) Atypical enzyme kinetics: their effect on in vitro-in vivo pharmacokinetic predictions and drug interactions, *Curr. Drug Metab. 4*, 341−346.
6. Ueng, Y. F., Kuwabara, T., Chun, Y. J., and Guengerich, F. P. (1997) Cooperativity in oxidations catalyzed by cytochrome P450 3A4, *Biochemistry 36*, 370−381.
7. Galetin, A., Clarke, S. E., and Houston, J. B. (2003) Multisite kinetic analysis of interactions between prototypical CYP3A4 subgroup substrates: midazolam, testosterone, and nifedipine, *Drug Metab. Dispos. 31*, 1108−1116.
8. Wang, R. W., Newton, D. J., Liu, N., Atkins, W. M., and Lu, A. Y. (2000) Human cytochrome P-450 3A4: in vitro drug-drug interaction patterns are substrate-dependent, *Drug Metab. Dispos. 28*, 360−366.
9. Korzekwa, K. R., Krishnamachary, N., Shou, M., Ogai, A., Parise, R. A., Rettie, A. E., Gonzalez, F. J., and Tracy, T. S. (1998) Evaluation of atypical cytochrome P450 kinetics with two-substrate models: evidence that multiple substrates can simultaneously bind to cytochrome P450 active sites, *Biochemistry 37*, 4137−4147.
10. Hutzler, J. M., Wienkers, L. C., Wahlstrom, J. L., Carlson, T. J., and Tracy, T. S. (2003) Activation of cytochrome P450 2C9-mediated metabolism: mechanistic evidence in support of kinetic observations, *Arch. Biochem. Biophys. 410*, 16−24.
11. Jefcoate, C. R. (1978) Measurement of substrate and inhibitor binding to microsomal cytochrome P-450 by optical-difference spectroscopy, *Methods Enzymol. 52*, 258−279.
12. Sligar, S. G., and Gunsalus, I. C. (1976) A thermodynamic model of regulation: modulation of redox equilibria in camphor monooxygenase, *Proc. Natl. Acad. Sci. U.S.A. 73*, 1078−1082.
13. Guengerich, F. P. (1983) Oxidation−reduction properties of rat liver cytochromes P-450 and NADPH-cytochrome p-450 reductase related to catalysis in reconstituted systems, *Biochemistry 22*, 2811−2820.
14. Backes, W. L., Sligar, S. G., and Schenkman, J. B. (1982) Kinetics of hepatic cytochrome P-450 reduction: correlation with spin state of the ferric heme, *Biochemistry 21*, 1324−1330.
15. Davydov, D. R., Kumar, S., and Halpert, J. R. (2002) Allosteric mechanisms in P450eryF probed with 1-pyrenebutanol, a novel fluorescent substrate, *Biochem. Biophys. Res. Commun. 294*, 806−812.
16. Yoon, M. Y., Campbell, A. P., and Atkins, W. M. (2004) "Allosterism" in the elementary steps of the cytochrome P450 reaction cycle, *Drug Metab. Rev. 36*, 219−230.
17. Harlow, G. R., and Halpert, J. R. (1998) Analysis of human cytochrome P450 3A4 cooperativity: construction and characterization of a site-directed mutant that displays hyperbolic steroid hydroxylation kinetics, *Proc. Natl. Acad. Sci. U.S.A. 95*, 6636−6641.
18. Hosea, N. A., Miller, G. P., and Guengerich, F. P. (2000) Elucidation of distinct ligand binding sites for cytochrome P450 3A4, *Biochemistry 39*, 5929−5939.
19. Gillam, E. M., Baba, T., Kim, B. R., Ohmori, S., and Guengerich, F. P. (1993) Expression of modified human cytochrome P450 3A4 in *Escherichia coli* and purification and reconstitution of the enzyme, *Arch. Biochem. Biophys. 305*, 123−131.
20. Omura, T., and Sato, R. (1964) The carbon monoxide-binding pigment of liver microsomes. II. solubilization, purification, and properties, *J. Biol. Chem. 239*, 2379−2385.
21. Hildebrandt, A., Remmer, H., and Estabrook, R. W. (1968) Cytochrome P-450 of liver microsomes-one pigment or many, *Biochem. Biophys. Res. Commun. 30*, 607−612.
22. Jung, C., Ristau, O., and Rein, H. (1991) The high-spin/low-spin equilibrium in cytochrome P-450- -a new method for determination of the high-spin content, *Biochim. Biophys. Acta 1076*, 130−136.
23. Ristau, O., Rein, H., Greschner, S., Janig, G. R., and Ruckpaul, K. (1979) Quantitative analysis of the spin equilibrium of cytochrome P-450 LM2 fraction from rabbit liver microsomes, *Acta Biol. Med. Ger. 38*, 177−185.
24. Shkumatov, V. M., Smettan, G., Ristau, O., Rein, H., Ruckpaul, K., Chaschin, V. L., and Akhrem, A. A. (1988) Quantitation of interaction between cytochrome P-450scc and adrenodoxin−analysis in the median UV-region by second derivative spectroscopy, *Chem.-Biol. Interact. 68*, 71−83.
25. Dawson, J. H., Andersson, L. A., and Sono, M. (1982) Spectroscopic investigations of ferric cytochrome P-450-CAM ligand complexes. Identification of the ligand trans to cysteinate in the native enzyme, *J. Biol. Chem. 257*, 3606−3617.
26. Orme-Johnson, N. R., and Orme-Johnson, W. H. (1978) Detection and quantitation of free cytochrome P-450 and cytochrome P-450 complexes by EPR spectroscopy, *Methods Enzymol. 52*, 252−257.
27. Segel, I. H. (1975) *Enzyme kinetics: behavior and analysis of rapid equilibrium and steady-state enzyme systems*, John Wiley & Sons, New York.
28. Yamazaki, H., Ueng, Y. F., Shimada, T., and Guengerich, F. P. (1995) Roles of divalent metal ions in oxidations catalyzed by recombinant cytochrome P450 3A4 and replacement of NADPH−cytochrome P450 reductase with other flavoproteins, ferredoxin, and oxygen surrogates, *Biochemistry 34*, 8380−8389.
29. Peisach, J., and Blumberg, W. E. (1970) Electron paramagnetic resonance study of the high- and low-spin forms of cytochrome P-450 in liver and in liver microsomes from a methylcholanthrene-treated rabbit, *Proc. Natl. Acad. Sci. U.S.A. 67*, 172−179.
30. Kumaki, K., Sato, M., Kon, H., and Nebert, D. W. (1978) Correlation of type I, type II, and reverse type I difference spectra with absolute changes in spin state of hepatic microsomal cytochrome P-450 iron from five mammalian species, *J. Biol. Chem. 253*, 1048−1058.
31. Cammer, W., Schenkman, J. B., and Estabrook, R. W. (1966) EPR measurements of substrate interaction with cytochrome P-450, *Biochem. Biophys. Res. Commun. 23*, 264−268.
32. Remmer, H., Schenkman, J., Estabrook, R. W., Sasame, H., Gillette, J., Narasimhulu, S., Cooper, D. Y., and Rosenthal, O. (1966) Drug interaction with hepatic microsomal cytochrome, *Mol. Pharmacol. 2*, 187−190.
33. Mitani, F., and Horie, S. (1969) Studies on P-450. VI. The spin state of P-450 solubilized from bovine adrenocortical mitochondria, *J. Biochem. (Tokyo) 66*, 139−149.
34. Cheng, S. C., and Harding, B. W. (1973) Substrate-induced difference spectral, electron paramagnetic resonance, and enzymatic properties of cholesterol-depleted mitochondrial cytochrome P-450 of bovine adrenal cortex, *J. Biol. Chem. 248*, 7263−7271.
35. Cinti, D. L., Sligar, S. G., Gibson, G. G., and Schenkman, J. B. (1979) Temperature-dependent spin equilibrium of microsomal and solubilized cytochrome P-450 from rat liver, *Biochemistry 18*, 36−42.
36. Renaud, J. P., Davydov, D. R., Heirwegh, K. P., Mansuy, D., and Hui Bon Hoa, G. H. (1996) Thermodynamic studies of substrate binding and spin transitions in human cytochrome P-450 3A4 expressed in yeast microsomes, *Biochem. J. 319* (Part 3), 675−681.
37. Fisher, M. T., and Sligar, S. G. (1987) Temperature jump relaxation kinetics of the P-450cam spin equilibrium, *Biochemistry 26*, 4797−4803.
38. Lewis, D. F. V. (2001) *Guide to Cytochromes P450: Structure and Function*, Taylor & Francis, New York.
39. Cupp-Vickery, J., Anderson, R., and Hatziris, Z. (2000) Crystal structures of ligand complexes of P450eryF exhibiting homotropic cooperativity, *Proc. Natl. Acad. Sci. U.S.A. 97*, 3050−3055.
40. Davydov, D. R., Halpert, J. R., Renaud, J. P., and Hui Bon Hoa, G. (2003) Conformational heterogeneity of cytochrome P450 3A4 revealed by high-pressure spectroscopy, *Biochem. Biophys. Res. Commun. 312*, 121−130.
41. Roberts, A. G., Bowman, M. K., and Kramer, D. M. (2004) The inhibitor DBMIB provides insight into the functional architecture of the Q_o site in the cytochrome b_6f complex, *Biochemistry 43*, 7707−7716.
42. Roberts, A. G., and Kramer, D. M. (2001) Inhibitor 'double-occupancy' in the Q_o pocket of the chloroplast cytochrome b_6f complex, *Biochemistry 40*, 13407−13412.

43. Davydov, D. R., Botchkareva, A. E., Kumar, S., He, Y. Q., and Halpert, J. R. (2004) An electrostatically driven conformational transition is involved in the mechanisms of substrate binding and cooperativity in cytochrome P450eryF, *Biochemistry 43*, 6475−6485.
44. He, Y. A., Roussel, F., and Halpert, J. R. (2003) Analysis of homotropic and heterotropic cooperativity of diazepam oxidation by CYP3A4 using site-directed mutagenesis and kinetic modeling, *Arch. Biochem. Biophys. 409*, 92−101.
45. Baas, B. J., Denisov, I. G., and Sligar, S. G. (2004) Homotropic cooperativity of monomeric cytochrome P450 3A4 in a nanoscale native bilayer environment, *Arch. Biochem. Biophys. 430*, 218−228.
46. Williams, P. A., Cosme, J., Vinkovic, D. M., Ward, A., Angove, H. C., Day, P. J., Vonrhein, C., Tickle, I. J., and Jhoti, H. (2004) Crystal Structures of Human Cytochrome P450 3A4 Bound to Metyrapone and Progesterone, *Science 305*, 683−686.
47. Fersht, A. (1995) *Enzyme Structure and Mechanism*, 2nd ed., W. H. Freeman and Company, New York.
48. Chen, Y. I., Chen, Y. H., Chou, W. Y., and Chang, G. G. (2003) Characterization of the interactions between Asp141 and Phe236 in the Mn^{2+}-l-malate binding of pigeon liver malic enzyme, *Biochem. J. 374*, 633−637.
49. Barrick, D. (2000) Trans-substitution of the proximal hydrogen bond in myoglobin: II. Energetics, functional consequences, and implications for hemoglobin allostery, *Proteins 39*, 291−308.
50. Kenworthy, K. E., Bloomer, J. C., Clarke, S. E., and Houston, J. B. (1999) CYP3A4 drug interactions: correlation of 10 in vitro probe substrates, *Br. J. Clin. Pharmacol. 48*, 716−727.
51. Schwab, G. E., Raucy, J. L., and Johnson, E. F. (1988) Modulation of rabbit and human hepatic cytochrome P-450-catalyzed steroid hydroxylations by alpha-naphthoflavone, *Mol. Pharmacol. 33*, 493−499.

BI0481390